Interference Localization from Space Theoretical Background

iStockphoto.com/enot-poloskun

Radio Frequency Interference causes the satellite industry to lose millions of dollars per year due to detrimental effects, ranging from a degradation in the quality of service to the complete loss of service. As a consequence, it is becoming critical important to design space systems that are able to localize the source of interference, allowing actions that can prevent future repetitions of similar behaviors. This is the first of a series of articles on the issue of interference localization. This article discusses the theoretical aspects associated with single-interferer localization approaches, describing how to extract those features providing information on the interference source location from the received interference signal itself, and how to compute a position fix by merging the collected information.

LUCA CANZIAN, STEFANO CICCOTOSTO, SAMUELE FANTINATO, ANDREA DALLA CHIARA, GIOVANNI GAMBA, OSCAR POZZOBON
QASCOM S.R.L.

RIGAS IOANNIDES, AND MASSIMO CRISCI
EUROPEAN SPACE AGENCY ESTEC

Radio frequency interference (RFI) represents a serious threat for the satellite industry. In satellite communications (SATCOM), though a small amount of satellite capacity is affected at any time by interference, 85–90 percent of the SATCOM customer issues are related to RFI (see M. Coleman in the Additional Resources section near the end of this article). According to the *Open 2015 SA Users Meeting General Forum,* this represents the single most important operational problem affecting customer service on geostationary satellites.
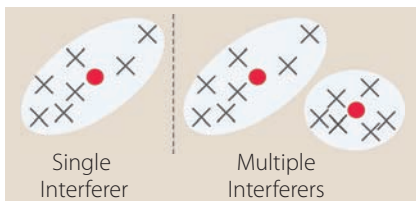
The majority of interference cases still come down to human error or equipment failure, with intentional interference (jamming) counting for less than five percent of interference cases. However, this is increasing dramatically. Detecting and localizing the source of RFI is becoming a priority in today's satellite industry generally and in the GNSS community in particular. Indeed, localization provides the required essential information to the authorities on the location of the RFI source and the time of such interference events, enabling them to take appropriate actions to eliminate such interference sources and prevent them from re-appearing.

This article discusses the theoretical background on interference localization, focusing on the single interferer case. The traditional approach to localize the source of an interference signal requires two steps:

1) generation of location measurements: first the interference signal must be processed in order to extract some features providing information on the interferer state (position and, possibly, velocity);

2) localization of the interference source: multiple collected measurements (generated simultaneously and/or at different time instants) are used as the inputs of a localization algorithm in order to generate an estimate of the interferer state.

Both steps are described in detail throughout the article, providing exam-

FIGURE 1 Single interferer localization (left side) and multiple interferer localization (right side). The crosses and red points represent the collected measurements and the interferer position estimates, respectively. All crosses within the same ellipse are assigned to the same estimated interferer.

ples of location measurement types and of techniques to estimate such location measurements and perform the final localization. A second article in this Working Papers series will appear in a subsequent issue of *Inside GNSS* and discuss the application of the techniques described here to GNSS interference localization. That article will present simulation results for both the ground and space GNSS interference localization architectures.

As an illustrative example, the left side of **Figure 1** depicts a set of location measurements, represented by black crosses, and the associated interferer location estimate, represented by a red point. In Figure 1, a single location measurement coincides with a point in the space, allowing us to simplify the representation; however, in general a location measurement defines a loci of points in the space, which we will discuss in more detail later in this article.

If multiple interferers are present and must be localized, an additional intermediate step is required: different location measurements must be assigned to different interferers, such that different subsets of the collected measurements are exploited to localize different interferers. The right side of Figure 1 illustrates this situation in which the total set of measurements is divided into two subsets, and two independent localizations are performed exploiting the two subsets of measurements.

There are many ways of splitting a set of n measurements into two subsets (precisely 2^{n-1} including the possibility of assigning all measurements to a single interferer). The situation gets worse if

the number of interferers is larger, and even worse if the number is unknown. Multiple-hypothesis tracking techniques jointly perform the assignation step (including the interferer number estimate, in cases where it is unknown) and the localization step, keeping in memory multiple assignation possibilities (named "hypotheses"). This results in multiple possibilities for the estimated number of interferers and the estimated location for each of them. We will not treat the case of multiple interferer localization here, but interested readers may learn more in the article by L. D. Stone *et alia* (Additional Resources).

Location Measurement Generation

The localization of an interferer requires the extraction of features from the inference signal providing information on the state (position and, possibly, velocity) of the interferer. We will now present a series of location-dependent measurements that can be obtained from an interfering signal.

A *time of arrival* (ToA) measurement represents the time a signal takes to travel from the transmitting source to the receiver (i.e., the propagation time), and can be written as:

$$ToA = \frac{\rho(x, y, z)}{c} + \epsilon$$

where $\rho(x, y, z)$ is the transmitter-to-receiver distance, which depends on the transmitter position *(x,y,z)*, c is the speed of light, and ϵ represents a possible measurement error.

All the points that are equidistant from the receiver are associated with the same ToA value as shown in the upper-left sub-figure of **Figure 2**, where the blue cross represents the transmitter position, the red triangle represents the receiver position, and the green circle is the ToA locus of points assuming $\epsilon = 0$. Because the ToA requires an accurate knowledge of the time at which the signal is transmitted, in the context of interferer localization we can generally not estimate such a measurement unless the signal itself contains a timing feature.

A *time difference of arrival* (TDoA) measurement represents the difference of the time instants at which a signal is

received at two different receivers, and can be written as:

$$TDoA = \frac{\rho_1(x, y, z) - \rho_2(x, y, z)}{c} + \epsilon$$

where $\rho_1(x, y, z)$ and $\rho_2(x, y, z)$ are the distances from the transmitter to the first and second receivers, respectively, which depend on the transmitter position *(x,y,z)*; c is the speed of light, and ϵ represents a possible measurement error.
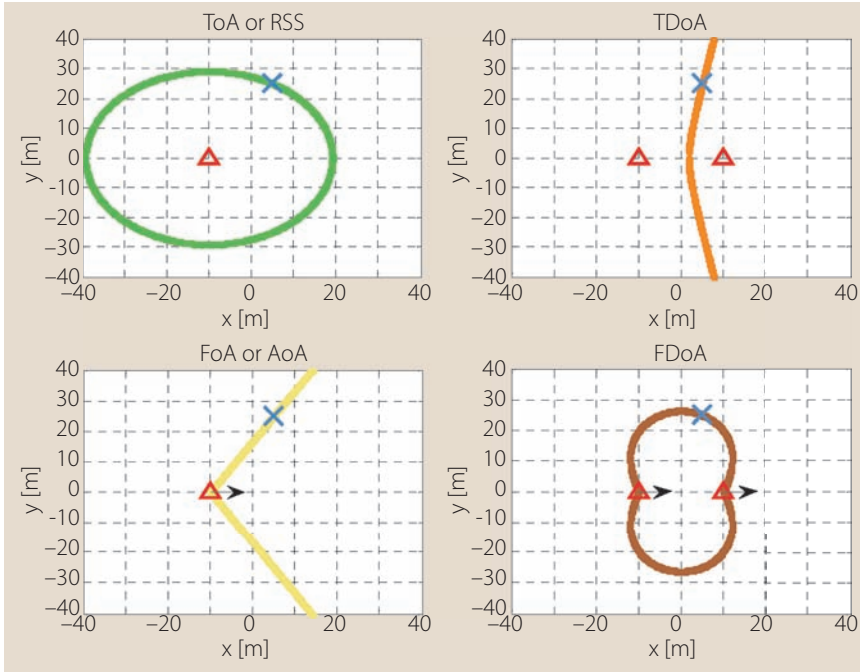
All the points such that the difference between the distances to each receiver is constant are associated with the same TDoA value. Hence, the locus of points satisfying a given TDoA measurement is a hyperbola in a two-dimensional space and a hyperboloid in a 3D space. The upper-right sub-figure of Figure 2 illustrates this measurement, where the blue cross is the transmitter position, the red triangles are the receiver positions, and the green circle is the TDoA locus of points assuming $\epsilon = 0$ (For details, see the article by Y. T. Chan and K. C. Ho in Additional Resources.)

A *frequency of arrival* (FoA) measurement represents the frequency shift (i.e., the Doppler) at which a signal is received by a receiver and can be written as:

$$FoA = \frac{f_0}{c} \|\mathbf{v}(x, y, z)\| \cos \alpha(x, y, z) + \epsilon$$

where $\mathbf{v}(x, y, z)$ is the relative speed vector between the receiver and the transmitter, $\alpha(x, y, z)$ is the angle between $\mathbf{v}(x, y, z)$ and the vector connecting the receiver to the transmitter, f_0 is the carrier frequency, c is the speed of light, and ϵ represents a possible measurement error.

In the case where the transmitter is static, the vector $\mathbf{v}(x, y, z)$ does not depend on the transmitter position *(x,y,z)*, and all the points with constant angle $\alpha(x, y, z)$ are associated with the same FoA value. Hence, in this case the locus of points satisfying a given FoA measurement is represented by two half-lines departing from the receiver position. It is symmetrical with respect to the receiver velocity in a 2D space and by a cone whose apex is the receiver position and axis is the receiver velocity in a 3D space. In the case where $\epsilon = 0$

FIGURE 2 Loci of points associated with ToA, TDoA, FoA, FDoA, RSS, and AoA measurements. The blue crosses are the transmitter positions, the red triangles are the receiver positions, and the black arrows represent either the receiver velocities (for FoA or FDoA), or reference directions (for AoA).

such a curve crosses the actual position of the transmitter.

The lower-left sub-figure of Figure 2 shows this situation, where the blue cross is the transmitter position, the red triangle is the receiver position, the black arrow is the receiver velocity, and the yellow half-lines represent the TDoA locus of points, assuming $\epsilon = 0$. Because the FoA requires an accurate knowledge of the signal carrier frequency (otherwise the Doppler cannot be subtracted from the received frequency), in the context of interferer localization we generally cannot estimate such a measurement.

A *frequency difference of arrival* (FDoA) measurement represents the difference between the frequency shifts (i.e., the Doppler) at which a signal is received by two different receivers and can be written as:

$$FDoA = \frac{f_0}{c} (\|\boldsymbol{v}_1(x,y,z)\| \cos \alpha_1(x,y,z) - \|\boldsymbol{v}_2(x,y,z)\| \cos \alpha_2(x,y,z)) + \epsilon$$

where $\boldsymbol{v}_1(x,y,z)$ and $\boldsymbol{v}_2(x,y,z)$ are the relative speed vectors between the two receivers and the transmitter, $\alpha_1(x,y,z)$ is the angle between $\boldsymbol{v}_1(x,y,z)$ and the vector connecting the first receiver to the transmitter (analogous to $\alpha_2(x,y,z)$, f_0 is the carrier frequency, c is the speed of light, and ϵ represents a possible measurement error. In the case of a static transmitter, the vectors $\boldsymbol{v}_1(x,y,z)$ and $\boldsymbol{v}_2(x,y,z)$ do not depend on the transmitter position *(x,y,z)*.

The locus of points of an FDoA measurement is not a standard geometric shape as seen in brown in the lower-right sub-figure of Figure 2 assuming $\epsilon = 0$, where the blue cross is the transmitter position, the red triangles are the receiver positions, and the black arrows are the receiver velocities. Note that

the exploitation of an FDoA measurement requires the knowledge of the carrier frequency (f_0 appears in the above equation); however, a small relative error on the carrier frequency estimation causes only a small perturbation of the locus of points.

A *received signal strength* (RSS) measurement represents the attenuation associated with the signal propagation from the transmitter to the receiver and can be written as:

$$RSS = 10 n_p \log_{10}(\rho(x,y,z)) + \epsilon$$

where $\rho(x,y,z)$ is the transmitter-to-receiver distance, which depends on the transmitter position *(x,y,z)*, n_p is the path loss factor, and ϵ represents a possible measurement error.

All the points that are equidistant from the receiver are ascribed the same RSS value. Hence, similarly to the ToA case, the locus of points satisfying a given RSS measurement is a circle in a 2D space (as shown by the upper-left sub-figure of Figure 2), and a sphere in a 3D space. Because the RSS requires an accurate knowledge of the power at which the signal is transmitted, in the context of interferer localization we generally cannot estimate such a measurement.

A *received signal strength difference* (RSSD) measurement represents the difference of the attenuations associated with the signal propagation from the transmitter to two different receivers, and can be written as:

$$RSSD = 10 n_p \log_{10}\left(\frac{\rho_1(x,y,z)}{\rho_2(x,y,z)}\right) + \epsilon_i$$

where $\rho_1(x,y,z)$ and $\rho_2(x,y,z)$ are the distances from the transmitter to the first and second receivers, respectively, which depend on the transmitter position *(x,y,z)*; n_p is the path loss factor, and ϵ represents a possible measurement error.

All the points whose ratio between the distances to each receiver is constant are associated with the same TDoA value. Hence, the locus of points satisfying a given RSSD measurement form a circle in a 2D space (a sphere in a 3D space), centered along the line connecting the two receivers and including only one of the two receivers, the one closer to the transmitter. If the transmitter is equidistant to the receivers, such a circle (sphere) degenerates to the line (plane) that is the perpendicular bisector to the segment connecting the two receivers. The RSSD requires an accurate knowledge of the path loss factor n_p. This factor is impacted by effects that are difficult to predict and compensate for, such as shadowing and multipath.

An *angle of arrival* (AoA) measurement represents the angle of the vector connecting a receiver to the transmitter with respect to a reference direction (in a 2D or 3D space) or a reference system (3D space). Denoting such an angle as $\alpha(x,y,z)$,

which is a function of the transmitter position (x,y,z), the AoA measurement can be written as:

$$AoA = \alpha(x, y, z) + \epsilon$$

where ϵ represents a possible measurement error.

If the AoA is computed with respect to a reference direction, the AoA locus of points is equivalent to the FoA locus of points: two half lines in a 2D space (as shown by in the lower-left sub-figure of Figure 2, where the black arrow represents in this case the reference direction), or a cone in a 3D space. If the AoA is computed with respect to a reference Cartesian system in a 3D space, then $\alpha(x, y, z)$ is actually a pair of angles, representing the azimuth and elevation with respect to the Cartesian system. In this case, the locus of points is a half-line departing from the reference position, or two half-lines if the sign of the elevation angle is uncertain.

Choosing and Generating the Measurement Types

In the context of interferer localization, because the information about the state of the signal at the transmitter is in general not available (e.g., transmitting time, transmitting power, carrier frequency), the most promising measurement types are the TDoA, FDoA, and AoA. We will now address possible signal processing to estimate such measurements.

A single TDoA measurement and a single FDoA measurement associated with a transmitter and a pair of receivers can be obtained by computing the *cross ambiguity function* (CAF) $\chi_{s,g}(\Delta t, \Delta f)$ between the signals $s(t)$ and $g(t)$ received by the two antennas during a common acquisition time interval $[t_1, t_1 + T]$ (as discussed in the paper by G. D. Hartwell in Additional Resources):

$$\chi_{s,g}(\Delta t, \Delta f) = \int_{t_1}^{t_1+T} s^*(t)g(t + \Delta t) e^{j2\pi\Delta f(t-t_1)} dt$$

The values Δt^* and Δf^* at which $\chi_{s,g}(\Delta t, \Delta f)$ is maximized represent the estimated TDoA and FDoA measurements, respectively. For a given value of Δf, the CAF is equivalent to a correlation between the signal $s(t)$ shifted in frequency by an amount Δf and the signal $g(t)$. As this correlation is in general performed after the signals are acquired and sampled, in practice the integral is actually a sum:

$$\chi_{s,g}(kT_s, \Delta f) = \sum_{t=n_1T_s}^{n_1T_s+K \cdot T_s} s^*(t)g(t + kT_s)e^{j2\pi\Delta f(t-n_1T_s)}$$

where T_s is the sampling time, $n_1 T_s$ is the beginning of the acquisition time interval, which corresponds to the time at which the TDoA measurement is evaluated, and $K \cdot T_s$ is the length of the acquisition time interval.

The foregoing function must be computed for a range of possible time and frequency shifts. For example, the TDoA cannot be larger, in absolute value, than the time a signal takes to travel from one antenna to the other, i.e., $|TDoA| \leq d/c$, where d is the distance between the two antennas and c is the speed of light. The CAF function can be fitted or interpolated in the
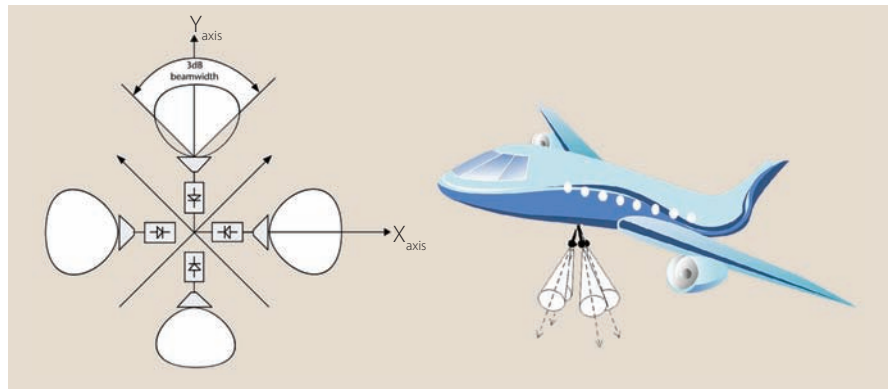

FIGURE 3 Possible arrangement of four antennas to implement the ACM technique, for a 2D space (left side, taken from A. De Martino) and for a 3D space (right side)

time domain in order to estimate the CAF peak with a time resolution that is better than the sampling time T_s.

We can obtain an AoA measurement in multiple ways. The most intuitive approach consists of taking and comparing amplitude measurements at different angles. This can either be performed by a single moving antenna scanning sequentially different angles, or by a set of fixed antennas that are oriented toward different angles. The latter approach is often referred to as *amplitude comparison monopulse* (ACM).

Figure 3 (left side) presents a possible planar architecture of the ACM technique, which is taken from A. De Martino (see Additional Resources). In this 2D example, four antennas are employed to estimate the AoA of a signal. Each antenna faces toward a specific quadrant. This means that the angle between the pointing directions of adjacent antennas, often referred to as the "squint angle," is 90 degrees. In this example, 90 degrees is also the three-decibel beamwidth of each antenna pattern, meaning that at least one antenna receives the signal within the three-decibel beamwidth of the main lobe. As a consequence, this antenna architecture covers a span of 360 degrees.

The AoA of the signal lies in the angular area between the antenna receiving the largest power and the antenna receiving the second largest power. This AoA can be obtained more accurately by computing the difference between these two received powers, and normalizing the results with respect to the sum of the two powers. If the antenna patterns and squint angle are properly designed, such a normalized difference is about linear with respect to the AoA (at least in the 90-degree angular span between the two antenna pointing directions). Hence, the AoA value can be unequivocally retrieved from the normalized difference. Smaller squint angles allow for achieving better accuracies, at the cost of requiring a larger number of antennas to cover the required angular span.

A similar approach can be adopted for a 3D space. In this case, in order to find both the azimuth and elevation angles with respect to an x-y-z Cartesian system, the antenna pointing directions must not lie in the same plane. The illustration on the right-hand side of Figure 3 shows a four-antenna implementation of the ACM technique to estimate the AoA of a signal coming from below of an airplane. In this representation, the four antennas are located at the same point and oriented to

four different angles covering a limited angular span. Note that antenna colocation is not a requirement, in particular if the interferer is located far below the airplane.

We can also derive the AoA from a TDoA measurement if the interferer is much farther away than the distance d separating the two receivers. Indeed, under this assumption the interferer signal can be approximated by a planar wave, which arrives at a certain angle with respect to the segment connecting the two receivers, and such an angle unequivocally defines the extra path that the signal must cover to reach the farther antenna.

Another way to realize that the TDoA is linked to the AoA for a far transmitter is by considering the fact that the hyperbola (hyperboloid), defining the locus of points of a TDoA measurement, has a linear (conical) asymptote, which corresponds to the locus of points of an AoA measurement. Mathematically, the AoA and the TDoA are linked by:

$$TDoA = \frac{d}{c}\sin AoA \xrightarrow{yields} AoA = \sin^{-1}\left(TDoA \cdot \frac{c}{d}\right)$$

Finally, there exist different techniques with which to exploit the phase of a narrowband signal transmitted by a far source and received by multiple receivers. This approach is similar in philosophy to the TDoA approach just described. Indeed, for a continuous signal (which is on the extreme of the narrowband signal class) a one-to-one correspondence exists between the differential time and the differential phase at which a signal is received at two receivers, assuming that the receiver separation is not larger than half a wavelength.

Among all the techniques exploiting the different phases of the signals acquired by multiple receivers, the most famous and widely adopted one is probably the MUltiple SIgnal Classification (MUSIC) technique (described in M. Hajian *et alia*). MUSIC was devised as a form of super-resolution direction-finding technique for processing the signals received by an antenna array of M antenna elements, to obtain estimates of the AoA of multiple signal components. It is in a family of processes called subspace-based processing and is based on an eigen-decomposition of the covariance matrix derived from data samples to obtain two orthogonal matrices, which represent the signal-subspace and the noise-subspace.

The MUSIC algorithm can be summarized as follows:
Step 1: Collect input samples $x(k)$ at multiple time instants $k = 1, \ldots, N$ and estimate the input covariance matrix

$$\hat{R}_{xx} = \frac{1}{N}\sum_{k=1}^{N} x(k).$$

Step 2: Perform eigen-decomposition of $\hat{R}_{xx}$ in order to get the M eigenvalues $\lambda_1 \geq \lambda_2 \geq \ldots \geq \lambda_M$ and the M associated eigenvectors $v_1, v_2 \ldots v_M$.
Step 3: Estimate the number of incident signals $\hat{D} = M - K$, where K is ideally the multiplicity of the smallest eigenvalue.

In practice, because $\hat{R}_{xx}$ is estimated

through a finite number of samples and therefore is affected by estimation errors, the eigenvalues will all be different. In this case K can be estimated as the number of small eigenvalues that are closely spaced.

Step 4: For each possible pair of angles of arrival (θ, ϕ), representing azimuth and elevation with respect to the reference Cartesian system, compute the MUSIC spectrum:

$$\hat{P}_{MUSIC}(\theta, \phi) = \frac{a^H(\theta, \phi)a(\theta, \phi)}{a^H(\theta, \phi)V_N V_N^H a(\theta, \phi)}$$

where $V_N = [v_{\hat{D}+1}, \ldots, v_M]$, $(\cdot)^H$, denotes the Hermitian transpose operator, $\alpha(\theta, \phi)$ is the "steering vector," which is given by:

$$a(\theta, \phi) = \begin{bmatrix} e^{-i\xi_1(\theta,\phi)} \\ e^{-i\xi_2(\theta,\phi)} \\ \vdots \\ e^{-i\xi_3(\theta,\phi)} \end{bmatrix}$$

and

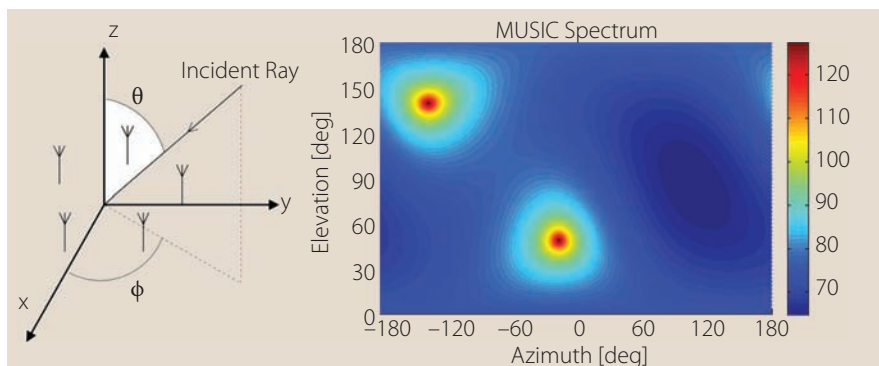$$\xi_i(\theta, \phi) = \frac{2\pi f}{c}(x_i\sin\theta\cos\phi + y_i\sin\theta\sin\phi + z_i\cos\theta)$$

is the phase shift observed by the i-th antenna with respect to the origin of the reference system, for an incoming wave with frequency f and incident angles (θ, ϕ).
Step 5: Find the $\hat{D}$ largest peaks of $\hat{P}_{MUSIC}(\theta)$ to obtain the estimates of the AoA of the incident signals.
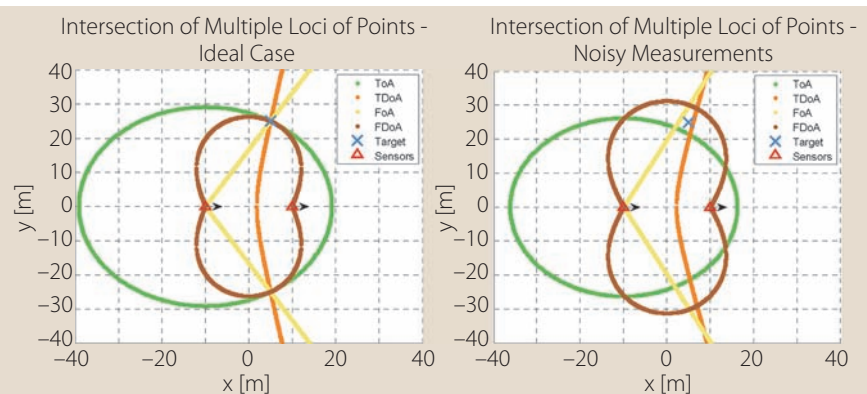
A common antenna arrangement for the MUSIC algorithm is the uniform circular array geometry in which the M antennas are placed along a circumference at equispaced distances. Such a disposition is shown for M = 5 antennas on the left side of **Figure 4**, and in this case the antennas represent the vertex of a pentagon.

It is important to note that, for a planar array, the MUSIC spectrum is symmetric with respect to the plane in which the antennas lie. As a consequence, a pair of peaks appears for each incident signal component: one is associated with the actual direction of arrival, while the other is a "ghost peak" (see right side of Figure 3), which must be somehow discarded.

In fact, to remove such ambiguity, the planar array should be placed such that no signal can reach the array from one of the two sub-spaces defined by the plane in which the antennas lie. In this case, we can limit the search for the MUSIC spectrum peaks to only the relevant sub-space and more specifically

FIGURE 4 Representation of the uniform circular array disposition (left side) and of the MUSIC spectrum in which both the actual peak and the ghost peak appear (right side).

FIGURE 5 Intersection of the loci of points associated with ToA (or RSS), TDoA, FoA (or AoA), and FDoA measurements, both in the ideal case (left side), and in the case where they are affected by errors (right side). The blue cross is the interferer position, the red triangles are the receiver positions, and the black arrows represent the receiver velocities.

to the relevant angles coming from the relevant subspace. (By limiting the field of view, we can also limit the angles at which we need to look.)

Localization

Figure 2 shows that a single location-dependent measurement does not allow for accurately localizing an interferer: all the points belonging to the loci of points of the measurement represent possible positions of the interferer. In order to resolve such ambiguity multiple location measurements are required. Such measurements may be collected simultaneously (e.g., N receivers collecting N-1 TDoA measurements), or sequentially at different instants (e.g., two receivers collecting a single TDoA every 10 seconds), or with both approaches (e.g., N receivers collecting N-1 TDoA measurements every second). Also, they may be of the same type or of different types (e.g., N receivers collecting N-1 TDoA and N-1 FDoA measurements every second).

Once a set of measurements is available, the goal of a localization technique is to find a point in the space that agrees with the observed measurements, with said point representing the estimate of the transmitter position. Geometrically, this is equivalent to finding the intersection of the loci of points associated with the measurements.

The left side of Figure 5 shows, in a unique picture, the loci of points that Figure 2 shows in different sub-figures. The ToA and FoA measurements refer only to the first receiver (two ToA and two FoA measurements could be taken by two receivers). In this specific scenario, all the loci intersect exactly at two points: one represents the actual interferer position, the other one is a point that is symmetric to the interferer position with respect to the x-axis. This symmetry occurs because both segments connecting the two receivers and the receiver velocities lie along the x-axis.

Unless prior knowledge on the interferer position allows for excluding all the subspace y < 0, this example shows the necessity of having a "heterogeneous geometry" (e.g., receivers not aligned in space, velocity vectors not aligned with respect to the segment connecting the receivers, and so forth) in order to avoid symmetric scenarios that may lead to ambiguities.

A fundamental point missing in the above discussion is that measurements are in general affected by errors. This means that the loci of points associated with the noisy measurements do not pass exactly through the actual interferer position, and they do not cross exactly on the same point.

This situation is represented on the right side of Figure 5. In this case the localization technique must find the point of the space that "best fits" the observed measurements. This concept of "fitting" is usually expressed, in mathematical terms, through a least-squares problem, which tries to minimize the sum of the squares of the distances of the loci of points from the estimated position. Geometrically, this means finding

a point in the space as close as possible to all the loci.

With more measurements available, the more precise the solution of such a least-squares problem will become. Moreover, if the accuracies associated with the collected measurements are available (e.g., if TDoA and FDoA measurements are affected by i.i.d. Gaussian errors with standard deviations σ_{TDoA} and σ_{FDoA}), we can weight each measurement appropriately by considering how much the loci of points of that measurement can oscillate around the actual interferer position. This requires rescaling each measurement type by an appropriate geometric factor and solving a weighted least-squares problem.

Multiple ad hoc solutions have been proposed and studied in the literature to aggregate specific types of measurements. See, for example, as cited in the Additional Resources section, M. Hajian *et alia* considered a two-stage maximum likelihood technique to aggregate TDoA measurements, I. Guvenc *et alia* studied an approximate maximum likelihood technique for TDoA and FDoA measurements to overcome the required computational burden by translating the non-convex problem to a convex function, and D. Musicki and W. Koch used a Gaussian mixture measurement filter approach to aggregate TDoA and FDoA measurements.

This article, instead of considering different ad hoc approaches, focuses on two general techniques that can be adopted to aggregate whatever measurements types are available. The first technique, the *Taylor Series* (TS), is a batch technique that is particularly useful when the target to locate is stationary or moving slowly. The second technique, the *extended Kalman filter* (EKF), is a sequential technique that is able to track the trajectory of a moving target, estimating both its position and its velocity.

Taylor Series Technique

The Taylor-Series (TS) estimation discussed by W. H. Foy (Additional Resources) (or Gauss-Newton interpolation) is an iterative scheme to compute the solution of a set of algebraic (in general non-linear) equations.

Figure 6 shows a schematic representation of the Taylor-series estimation techniques applied to interference localization. It receives as input a set of location measurements m_i, $i = 1, \dots, n$, with the associated error covariance matrix R, and it outputs a position estimate $(\hat{x}, \hat{y}, \hat{z})$ along with the covariance matrix Q associated with such position estimate. To do so, TS starts with a rough initial guess of the position estimate and iteratively improves it by determining local corrections, until the algorithm converges.

The first step of this iterative approach consists of *rescaling* the location measurements m_i, $i = 1, \dots, n$, and the error covariance matrix R, to obtain the rescaled measurements $\tilde{m}_i$, $i = 1, \dots, n$, and the rescaled error covariance matrix $\tilde{R}$. The rescaling process consists of multiplying each location measurement by a factor that takes into account how far the locus of points of that location measurement would be from the interferer position in the case where that measurement is affected by a unit error.

If the location measurements are of different types, this procedure is particularly effective in order to weight the measurement errors properly, expressing everything in terms of distances. Because the rescaling factor depends on the interferer position, the rescaling process must be performed at every iteration, whenever a new position estimate is generated.

A rescaled location measurement can be expressed in the following way:

$$\tilde{m}_i = f_i(x, y, z) + \tilde{\epsilon}_i$$

where $f_i(x,y,z)$ is the function defining how the rescaled measurement $\tilde{m}_i$ is connected to the state (x,y,z); x,y,z are the true (unknown) coordinates of the interference source; $\tilde{\epsilon}_i$ is the error of the i-th rescaled measurement; and the vector $\tilde{\epsilon} = [\tilde{\epsilon}_1, \dots, \tilde{\epsilon}_n]^T$ is assumed to be a zero mean multivariate Gaussian noise with covariance $\tilde{R}$.

The subsequent step consists of *linearizing* (through a first-order expansion) the functional forms of the rescaled measurements around the current position estimate, obtaining the following matricial equation, which approximates well the real one around the current position estimate:

$$A \cdot \delta = z - \tilde{\epsilon}$$

where

$$A = \begin{bmatrix} a_{1x} & a_{1y} & a_{1z} \\ a_{2x} & a_{2y} & a_{2z} \\ a_{3x} & a_{3y} & a_{3z} \\ & \vdots & \\ a_{nx} & a_{ny} & a_{nz} \end{bmatrix} \; ; \quad \delta = \begin{bmatrix} \delta_x \\ \delta_y \\ \delta_z \end{bmatrix} \; ; \quad z = \begin{bmatrix} z_1 \\ z_2 \\ z_3 \\ \vdots \\ z_n \end{bmatrix} \; ; \quad \tilde{\epsilon} = \begin{bmatrix} \tilde{\epsilon}_1 \\ \tilde{\epsilon}_2 \\ \tilde{\epsilon}_3 \\ \vdots \\ \tilde{\epsilon}_n \end{bmatrix}$$

$$a_{ix} = \partial f_i / \partial x \big|_{\hat{x}, \hat{y}, \hat{z}} \; ; \quad a_{iy} = \partial f_i / \partial y \big|_{\hat{x}, \hat{y}, \hat{z}} \; ; \quad a_{iz} = \partial f_i / \partial z \big|_{\hat{x}, \hat{y}, \hat{z}} \; ;$$

$$z_i = \tilde{m}_i - f_i(\hat{x}, \hat{y}, \hat{z})$$

Next, the solution $\hat{\delta} = [\hat{\delta}_x \quad \hat{\delta}_x \quad \hat{\delta}_x]^T$ of the matricial equation $A \cdot \delta = z$ must be computed. The solution represents the correction term to apply to the current position estimate in order to improve it (locally). The matricial equation $A \cdot \delta = z$ is in general overdetermined; hence, the solution $\hat{\delta}$ must be computed with respect to a certain criterion, considering also the statistic of the errors affecting the location measurements. A commonly adopted criterion is the minimization of the squared Mahalanobis length of the residual vector, whose solution is given by the *generalized least square* method:

$$\hat{\delta} = argmin_\delta \ (z - A\delta)^T \tilde{R}^{-1}(z - A\delta) \xrightarrow{yields}$$

$$\hat{\delta} = \left[A^T \tilde{R}^{-1} A\right]^{-1} A^T \tilde{R}^{-1} z$$

Note that, for independent errors, this is equivalent to a weighted least-squares method, which minimizes the sum-squared error with the terms in the sum that are weighted according to the inverse of the corresponding error variances (hence giving more importance to more accurate measurements). Further, if the errors are also identically distributed then it is equivalent to a least-squares method.

Exploiting the correction term $\hat{\delta}$, the new position estimate is simply given by:

$$\begin{bmatrix} \hat{x} \\ \hat{y} \\ \hat{z} \end{bmatrix} \leftarrow \begin{bmatrix} \hat{x} \\ \hat{y} \\ \hat{z} \end{bmatrix} + \begin{bmatrix} \delta_x \\ \delta_y \\ \delta_z \end{bmatrix}$$
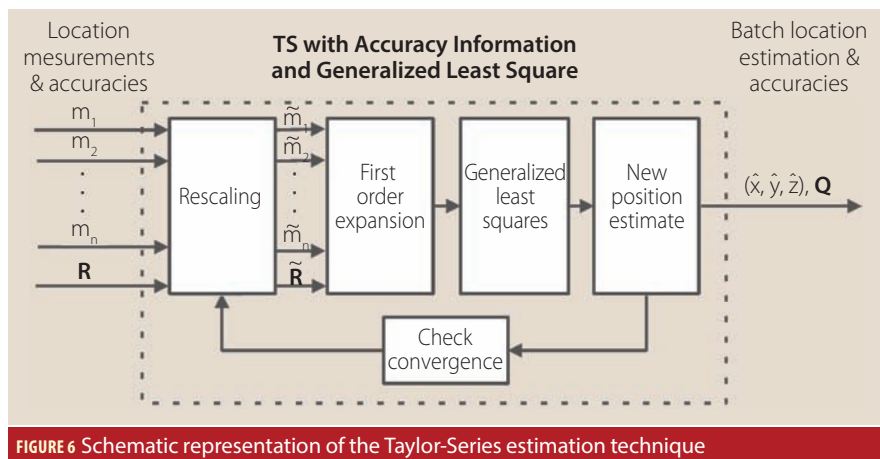
where $(\hat{x}, \hat{y}, \hat{z})$ is the current position estimate and the arrow represents the assignment operator.

These steps must be performed at each iteration until the algorithm converges. To check the convergence, it is possible to look at the correction term:

$$\left\| \hat{\delta} \right\| = \sqrt{\delta_x^2 + \delta_y^2 + \delta_z^2}$$

If $\left\| \hat{\delta} \right\|$ is smaller than a pre-selected threshold, the algorithm has converged. Conversely, if $\left\| \hat{\delta} \right\|$ is large and decreases after some iterations or if a maximum number of iterations is reached, then the algorithm fails to converge.

Significantly, the TS estimation technique converges to a local maxima of the

FIGURE 6 Schematic representation of the Taylor-Series estimation technique

original problem. Hence, although experience indicates that the initial position guess can be quite far off without preventing good convergence, it may be convenient to perform the TS estimation technique multiple times with different initial positions, and maintain the solution that best agrees with the observed measurements.

Finally, it is worth noting that the generalized least square method also provides the covariance matrix Q of the errors of the position estimate:

$$Q = \left[A^T \tilde{R}^{-1} A\right]^{-1} := \begin{bmatrix} \sigma_x^2 & \sigma_{xy} & \sigma_{xz} \\ \sigma_{xy} & \sigma_x^2 & \sigma_{yz} \\ \sigma_{xz} & \sigma_{yz} & \sigma_z^2 \end{bmatrix}$$

Q gives the statistics of the position estimate. For example, with the assumption that the error distribution is Gaussian, the η-confidence set of the position estimate (i.e., the smallest volume set that includes the real interferer position with a probability of at least η) is given by the ellipsoid centered in $(\hat{x}, \hat{y}, \hat{z})$ with the semiaxes given by $\sqrt{\alpha \lambda_i} \cdot u_i$, where, α is the value at which the cumulative density function of a chi-squared distribution with three degrees of freedom is equal to η, and u_i are (orthonormal) eigenvectors of Q with eigenvalues λ_i.

Alternatively, it is possible to transform the uncertainty Q expressed in the XYZ coordinates into the corresponding uncertainty in the East, North and Up (ENU) coordinates (in case the XYZ system is not already aligned with the ENU system), and then compute the horizontal and vertical position accuracies. Let T be the transformation matrix of ENU coordinates to XYZ, whose columns are the orthonormal vectors **e, n, u** expressed in the XYZ coordinate system at the point of longitude ϕ and latitude φ corresponding to the position estimate:

$$T = \begin{bmatrix} -\sin\phi & -\sin\varphi\cos\phi & \cos\varphi\cos\phi \\ \cos\phi & -\sin\varphi\sin\phi & \sin\varphi\sin\phi \\ 0 & \cos\varphi & \sin\varphi \end{bmatrix}$$

hence,

$$Q_{ENU} = T^T Q T := \begin{bmatrix} \sigma_E^2 & \sigma_{EN} & \sigma_{NU} \\ \sigma_{EN} & \sigma_N^2 & \sigma_{EU} \\ \sigma_{NU} & \sigma_{EU} & \sigma_U^2 \end{bmatrix}$$

where σ_E, σ_N, and σ_U define the accuracies toward the east, north, and vertical directions, respectively; $\sigma_H = \sqrt{\sigma_E^2 + \sigma_N^2}$ defines the accuracy in the horizontal plane, and

$$\sigma_{3D} = \sqrt{\sigma_E^2 + \sigma_N^2 + \sigma_U^2}$$

defines the accuracy in the tridimensional space. σ_U and σ_H are also known as vertical dilution of precision and horizontal dilution of precision, respectively. σ_H is the radius of the circle in the East-North plane that contains the real position with probability 0.65, whereas $2 \cdot \sigma_H$ is the radius of the circle that contains the real position with probability 0.95.

Other useful measures are the circular error probable (CEP) and the spherical error probable (SEP), which are the radius of the circle and of the sphere, respectively, that include the real position with probability 0.5. They are computed as
CEP $= 0.62 \cdot \sigma_E + 0.56 \cdot \sigma_N$
for $\sigma_N > \sigma_E$. Note that the roles are inverted for $\sigma_N, > \sigma_E$, and
SEP $= 0.51 \cdot (\sigma_E + \sigma_N + \sigma_U)$.

Extended Kalman Filter Technique

The extended Kalman filter (EKF) is the non-linear version of the Kalman filter, in which non-linearities are approximated by a linearized version around the current state estimate. It is a sequential technique that produces estimates of unknown variables by using Bayesian inference. This means that it keeps in memory a state estimate $\hat{x}_k$ and the uncertainty associated with said state estimate, quantified by a covariance matrix P_k (the subscript k is used to denote a specific time instant).

Further, whenever new measurements (with the associated accuracies) are available, the state estimate and the associated uncertainty are updated, exploiting the additional information carried by the new measurements. The EKF must be initialized with an initial state estimate with the associated uncertainty.

Figure 7 shows a schematic representation of the EKF estimation techniques applied to interference localization. At time instant k the EFK receives as input a set of location measurements $m_{i,k}$, $i = 1, \dots, n$, with the associated error covariance matrix R_k, and outputs a position estimate $\hat{x}_k$ along with the covariance matrix P_k associated with the position estimate. The subscript k, representing the current time instant, is used to flag the fact that the EKF technique is sequential: the current estimate depends both on the new measurements and on the previous estimate performed at time instant k–1.

As with the TS technique, the first step of the EKF technique involves rescaling the location measurements such that measurements of different types are weighted properly. Such rescaled measurements are then aggregated with the last state estimate performed by the EKF technique.

The model the EKF is based on is described by the following two equations:

$$x_k = h(x_{k-1}) + w_k$$
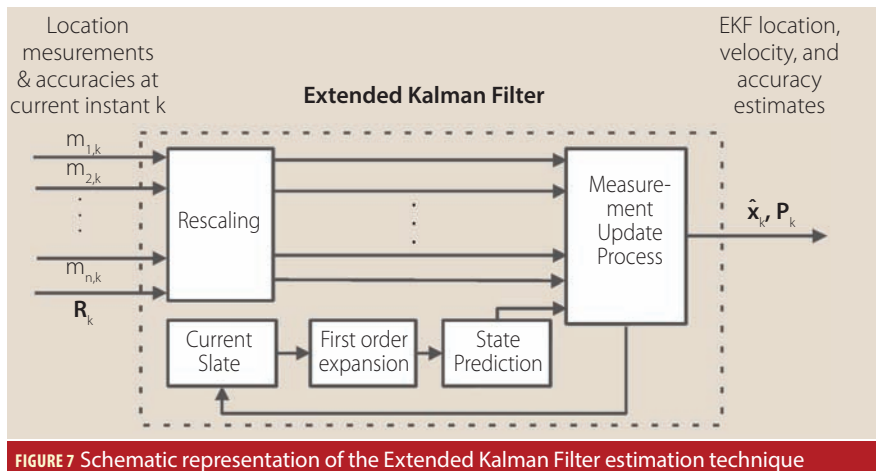$$\tilde{m}_{i,k} = f_i(x_k) + \tilde{\epsilon}_{i,k}$$

FIGURE 7 Schematic representation of the Extended Kalman Filter estimation technique

where x_k is the real current state to estimate, $h(\cdot)$ is the function defining how the state evolves in time, w_k is a noisy term that takes into account that the real state evolution may not follow exactly the deterministic model defined by the function $h(\cdot)$, w_k is assumed to be zero mean multivariate Gaussian noise with covariance Q_k; $\tilde{m}_{i,k}$ is the i-th current rescaled measurement; $f_i(\cdot)$ is the function defining how the current i-th rescaled measurement $\tilde{m}_{i,k}$ is connected to the current state x_k; and,

$\tilde{\epsilon}_{i,k}$ is the error of the i-th rescaled measurement, with the vector $\tilde{\boldsymbol{\epsilon}}_k = \left[\tilde{\epsilon}_{1,k}, \dots, \tilde{\epsilon}_{n,k}\right]^T$ assumed to be zero mean multivariate Gaussian noise with covariance $\tilde{R}_k$, which is obtained by rescaling the covariance matrix R_x.

In the context of interference localization, the state estimate x_k includes the position of the interferer and possibly its velocity if the interferer might be dynamic. In this case, the function $h(\cdot)$ represents the (assumed) motion model.

The current state estimate $\hat{x}_k$ is obtained from the previous state estimate $\hat{x}_{k-1}$ and the current rescaled measurements $\tilde{m}_k = \left[\tilde{m}_{1,k}, \dots \tilde{m}_{n,k}\right]^T$ through the following two steps, which are graphically represented in **Figure 8**:

Prediction step: The previous state estimate $\hat{x}_{k-1}$ is propagated up to the current time instant exploiting the motion model, obtaining:

$$\hat{x}_{k|k-1} = h(\hat{x}_{k-1})$$
$$P_{k|k-1} = H_{k-1}P_{k-1}H_{k-1}^T + Q_k$$

where:

$\hat{x}_{k|k-1}$ denotes the state estimate at step k obtained before exploiting the new measurements m_k;

$P_{k|k-1}$ is the covariance matrix associated to $\hat{x}_{k|k-1}$; and,
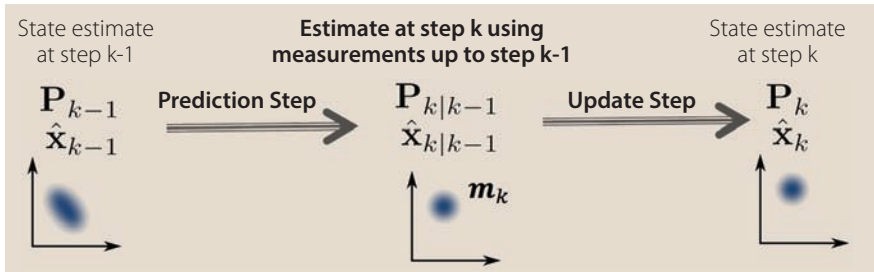
H_{k-1} if the Jacobian of the function $h(\cdot)$ in

$$\hat{x}_{k-1}: H_{k-1} = \left. \partial h(x)/\partial x \right|_{\hat{x}_{k-1}} :$$

Measurement update step: The predicted state estimate is merged with the new observed measurements, obtaining the final state estimate:

$$\hat{x}_k = \hat{x}_{k|k-1} + K_k v_k$$
$$P_{k|k}^E = P_{k|k-1} - K_k S_k K_k^T$$

where:

State estimate at step k-1 — Estimate at step k using measurements up to step k-1 — State estimate at step k

P_{k-1}, $\hat{x}_{k-1}$ — **Prediction Step** → $P_{k|k-1}$, $\hat{x}_{k|k-1}$ — **Update Step** → P_k, $\hat{x}_k$

m_k

FIGURE 8 Graphical representation of the EKF two-step approach to compute a new state estimate from the previous state estimate and the current measurements.

$\boldsymbol{v}_k = \left[v_{1,k}, \dots, v_{n,k}\right]^T$ is the measurement residuals computed with respect to the predicted state:

$$v_{i,k} = \tilde{m}_{i,k} - f_i(\hat{x}_{k|k-1});$$

K_k is the Kalman gain matrix:

$$K_k = P_{k|k-1}F_k'S_k^{-1};$$

F_k is the Jacobian of the function $f(\cdot)$ in the predicted state

$$\hat{x}_{k|k-1}: F_k = \left. \partial f(x)/\partial x \right|_{\hat{x}_{k|k-1}}$$

S_k is the innovation covariance:

$$S_k = F_k P_{k|k-1} F_k^T + \tilde{R}_k.$$

Conclusions and Future Work

This article discussed the theoretical aspects associated with single-interferer localization approaches, describing how to extract different types of location measurements from the received interference signal and how to compute a position fix by aggregating the collected location measurements.

We focused on two techniques to aggregate the collected location measurements: the Taylor Series and the extended Kalman filter techniques. The former is a batch and iterative scheme to compute the solution of a set of algebraic equations, starting with a rough initial guess of the position estimate and iteratively improving it by determining local corrections. The latter is a sequential technique that produces estimates of unknown variables by using Bayesian inference, keeping in memory a state estimate that is updated as soon as a new location measurement is available. Both techniques have the great advantage that they can incorporate heterogeneous types of location measurements, weighting each measurement appropriately.

The application of the techniques discussed in this article to GNSS interference localization will be examined in a subsequent Working Papers column, which will present simulation results for both the ground and space GNSS interference localization architectures. In addition to this follow-on article, the authors are currently working on developing and analyzing multiple hypothesis tracking techniques for space systems that are required to detect and localize multiple sources of interference.

Additional Resources

[1] Canzian, L., and S. Ciccotosto, S. Fantinato, A. Dalla Chiara, G. Gamba, O. Pozzobon, R. Ioannides, and M. Crisci, "Interference Localization from Space: Application," to appear in *Inside GNSS*

[2] Chan, Y. T., and K. C. Ho, "A Simple and Efficient Estimator for Hyperbolic Location," *IEEE Transaction in Signal Processing,* Volume: 42, Issue: 8, August 1994

[3] Coleman, M., "Satellite Interference - Issues of Concern," *Talk Satellite - EMEA,* <http://www.talk-satellite.com/EMEA-A27812.htm>, June 23, 2014

[4] De Martino, A., *Introduction to Modern EW Systems,* Artech House, 2012

[5] Einicke, G. A., "Smoothing, Filtering and Prediction: Estimating the Past, Present and Future," *Intech,* 2012

[6] Foy, W. H., "Position-Location Solutions by Taylor-Series Estimation," *IEEE Transactions on Aerospace and Electronic Systems,* Volume: AES-12, Issue: 2, 1976

[7] Guvenc, I., and Y. T. Chan, H. Y. C. Hang, and P. C. Ching, "Exact and Approximate Maximum Likelihood Localization Algorithms," *IEEE Transaction on Vehicular Technology,* Volume: 55, Issue: 1, January 2006

[8] Hajian, M., and C. Coman, and L. P. Ligthart, L. P., "Comparison of Circular, Uniform- and non-Uniform Y-Shaped Array Antenna for DOA Estimation using Music Algorithm," *2006 European Conference on Wireless Technology,* Manchester, 2006

[9] Hartwell, G. D., "Improved Geo-Spatial Resolution Using a Modified Approach to the Complex Ambiguity Function (CAF)," Thesis, Naval Postgraduate School, Monterey, CA, September 2005

[10] Jakhu, R. S., "Satellites: Unintentional and Intentional Interference," *Radio Frequency Interference and Space Sustainability,* June 2013

[11] Musicki, D. and Koch, W., "Geolocation using TDOA and FDOA measurements," *11th International Conference on Information Fusion,* Cologne, 2008

[12] *Open 2015 SDA Users Meeting General Forum,* <http://www.spacedata.org/sda/resources/briefings/>

[13] Poisel, R. A., *Electronic Warfare Target Location Methods,* Artech House, 2012

[14] Schmidt, R., "Multiple Emitter Location and Signal Parameter Estimation," *IEEE Transactions on Antennas and Propagation,* Volume: AP-34, Issue: 3, March 1986

[15] Stone, L. D., and R. L. Streit, T. L. Corwin, and K. L. Bell, *Bayesian Multiple Target Tracking,* 2nd Ed., Artech House, 2014

Authors

Luca Canzian has been a radio communication engineer at Qascom since April 2015. He received his master and Ph.D. degrees in electrical engineering from the University of Padova and has worked as a postdoctoral researcher on data mining techniques at the University of California Los Angeles and at the University of Birmingham. Since joining Qascom he has been involved in the Ground to Space Threat Simulator ESA project, and his main activity has focused on the design and evaluation of satellite-based interference geolocation techniques.

Samuele Fantinato is a radio navigation systems engineer at Qascom. He leads several projects with focus on the design of advanced radio navigation testbeds for interference, spoofing mitigation, and assessment of authentication schemes for GNSS. He holds a Master's degree in telecommunication engineering from the University of Padova.

Stefano Ciccotosto is a signal processing engineer at Qascom. He received a Master's degree in telecommunication Eeneering from the University of Padova. He is responsible for the design and testing of interference processing techniques.

Andrea Dalla Chiara is a designer and project manager at Qascom, with a focus on GNSS simulators, receivers, and authentication techniques both at the signal and data level. He is an electronic engineer, and has a Ph.D. in information technologies from the University of Padova.

Giovanni Gamba is an R&D engineer for Qascom. He is involved in theoretical design and development of interference and spoofing detection, mitigation, and localization algorithms for various GNSS-related projects. He holds a Ph.D. degree in information engineering from the University of Padova.

Oscar Pozzobon is the founder and technical director of Qascom. He received a degree in information technology engineering from the University of Padova in 2001 and a master degree from the University of Queensland in telecommunication engineering in 2003. He is coordinating different activities in the domain of interference, signal authentication and advanced navigation with the European Space Agency (ESA), the European GNSS Agency (GSA), the European Commission (EC) and the National Aeronautics and Space Administration (NASA). His main interests are GNSS, telecommunications and cryptography, where he holds more than 30 publications and 3 patents.

Rigas T. Ioannides works at the TEC-ETN section in the RF Payload Systems Division at ESA-ESTEC in support of radionavigation activities and the Galileo project. His main research interests include GNSS signal design, signal processing techniques for stand-alone and integrated hybrid GNSS architectures, authentication and anti-jamming techniques at system and user level for GNSS applications, and GNSS integrity concepts. Ioannides holds a Ph.D. in trans-ionospheric propagation effects on GNSS signals, and a M.Sc. degree in communications and real-time electronic systems from the University of Bradford.

Massimo Crisci is head of the Radio Navigation Systems and Techniques Section at the European Space Agency. He is the technical domain responsible for the field of radio-navigation. This responsibility encompasses radionavigation sys¬tems for satellite, aeronautical, maritime, and land mobile users (including indoor) applications, future radionavigation equipment/techniques/receivers for (hybrid satellite/ terrestrial) naviga¬tion/localization systems for ground and space applications, signal-in-space design, and end-to-end performance analysis for current and future radionavigation systems. Crisci is the head of a team of engineers providing radionavigation expert support to the various ESA programs (EGNOS and Galileo included). He holds a Ph.D. in automatics and operations research from the University of Bologna and a Master's degree in electronics engineering from the University of Ferrara.

Prof.-Dr. Günter Hein serves as the editor of the Working Papers column. He served as the head of the EGNOS and GNSS Evolution Program Department of the European Space Agency and continues to advise on scientific aspects of the Navigation Directorate as well as being a member the ESA Overall High Level Science Advisory Board. Previously, he was a full professor and director of the Institute of Geodesy and Navigation at the Universität der Bundeswehr München (UniBW), where he is now an ""Emeritus of Excellence." In 2002, he received the Johannes Kepler Award from the U.S. Institute of Navigation (ION). He is one of the inventors of the CBOC signal. **IG**